Quaternary International 487 (2018) 43–53

Contents lists available at ScienceDirect

Quaternary International

journal homepage: www.elsevier.com/locate/quaint

Climate changes reconstructed from a glacial lake in High Central Asia over the past two millennia

Jianghu Lan [a, *], Hai Xu [b, **], Enguo Sheng [c], Keke Yu [d], Huixian Wu [a, e], Kangen Zhou [a, e], Dongna Yan [a, e], Yuanda Ye [a, e], Tianli Wang [a, e]

[a] State Key Laboratory of Loess and Quaternary Geology, Institute of Earth and Environment, Chinese Academy of Sciences, Xi'an 710061, China
[b] Institute of Surface-Earth System Science, Tianjin University, Tianjin 300072, China
[c] State Key Laboratory of Environmental Geochemistry, Institute of Geochemistry, Chinese Academy of Sciences, Guiyang 550002, China
[d] Key Laboratory of Disaster Monitoring and Mechanism Simulating of Shaanxi Province, Baoji University of Arts and Sciences, Baoji 721013, Shaanxi, China
[e] University of Chinese Academy of Sciences, Beijing 100049, China

ARTICLE INFO

Article history:
Received 3 July 2017
Received in revised form
4 October 2017
Accepted 30 October 2017
Available online 20 November 2017

Keywords:
High Central Asia
Lake Harnur
Climate change
Westerlies
Over the past two millennia

ABSTRACT

Climatic changes in Arid Central Asia (ACA) over the past two millennia have been widely concerned. However, less attention has been paid to those in the High Central Asia (HCA), where the Asian water tower nurtures the numerous oases by glacier and/or snow melt. Here, we present a new reconstruction of the temperature and precipitation change over the past two millennia based on grain size of a well-dated glacial lake sediment core in the central of southern Tianshan Mountains. The results show that the glacial lake catchment has experienced cold-wet climate conditions during the Dark Age Cold Period (~300–600 AD; DACP) and the Little Ice Age (~1300–1870 AD; LIA), whereas warm-dry conditions during the Medieval Warm Period (~700–1270 AD; MWP). Integration of our results with those of previously published lake sediment records, stalagmite $\delta^{18}O$ records, ice core net accumulation rates, tree-ring based temperature reconstructions, and mountain glacier activities suggest that there has a broadly similar hydroclimatic pattern over the HCA areas on centennial time scale during the past two millennia. Comparison between hydroclimatic pattern of the HCA and that of the ACA areas suggests a prevailing 'warm-dry and cold-wet' hydroclimatic pattern over the whole westerlies-dominated central Asia areas during the past two millennia. We argue that the position and intensity of the westerlies, which are closely related to the phase of the North Atlantic Oscillation (NAO), and the strength of the Siberian High pressure (SH), could have jointly modulated the late Holocene central Asia hydroclimatic changes.

1. Introduction

Global warming since the mid-19th century has been well recognized (IPCC, 2007; Moberg et al., 2005; PAGES 2k Consortium, 2013; Neukom et al., 2014), but hydrological response shows a spatial heterogeneity (Chen et al., 2015; Xu et al., 2016). Owing to the limit of instrumental records, the knowledge of climate changes and its mechanisms during the late Holocene, especially over the past two millennia, are crucial for understanding the contemporary climate dynamics, predicting possible climate changes in future, and researching the past global climate changes. Numerous studies have been carried out to shed light on the climate changes over the past two millennia based on variable proxy indices (Diaz et al., 2011; Graham et al., 2011; PAGES 2k Consortium, 2013; Neukom et al., 2014; Schurer et al., 2014; Sigl et al., 2015; Xu et al., 2016), which have largely improved our understanding of the details in climatic changes and the related mechanisms. However, hydroclimatic changes and impacts are variable among different regions, and the mechanisms are not fully understood; further research on spatial-temporal pattern of different regions is necessary.

As one of the most arid areas in the world, central Asia is primarily dominated by the westerlies, and its climatic change and dynamic mechanisms have been widely concerned (Aizen et al., 1997, 2001, 2006; Yang et al., 2009; Chen et al., 2010; Cheng et al., 2012; Song et al., 2015). However, investigation of climatic

* Corresponding author.
** Corresponding author.
E-mail addresses: lanjh@ieecas.cn (J. Lan), xuhai2003@263.net (H. Xu).

https://doi.org/10.1016/j.quaint.2017.10.035
1040-6182/

change under global warming is seriously impeded by the limit of the instrumental record. Furthermore, the limited paleoclimate archives are mostly located at low-elevated areas (Chen et al., 2006, 2010; Sorrel et al., 2006; Kroonenberg et al., 2007; Huang et al., 2011; Ma et al., 2011). A series of mountains (e.g., Tianshan Mt., Altai Mt., and Pamir Plateau) are located at the central Asia; and the climate over those mountainous regions may be largely different with that of the low-elevated ACA areas. Because of the scarce of well-dated high resolution paleoclimate records in the HCA areas over the past two millennia, development of the geological proxies for temperature and precipitation records covering longer time spans would be a significant step forward for understanding of the climate changes over the HCA and their relationship with those over the ACA areas.

Here we reconstruct climatic changes over the past two millennia at Lake Harnur, a glacial lake of the central Tianshan Mt., based on ^{137}Cs, ^{210}Pb, AMS ^{14}C dating and sedimentary grain size analysis. We focus on hydroclimatic pattern in the HCA areas, and compare them with those over the extended ACA areas, and finally discuss the possible driving forces.

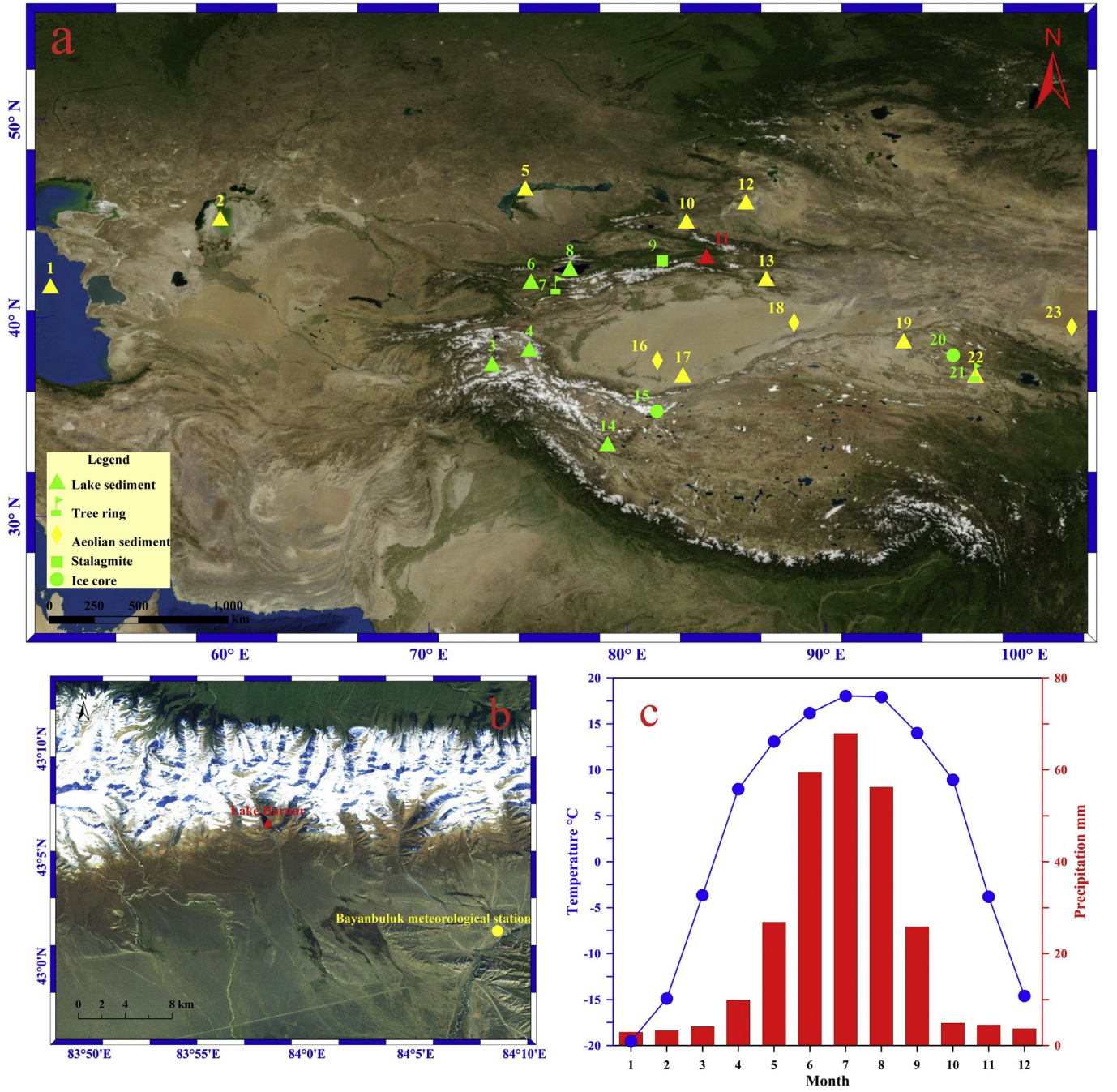

Fig. 1. (a) Locations of Lake Harnur (red triangle) and other sites (see numbers of other sites in Table 1) mentioned in the text. The green color sites note the HCA and the yellow sites present the ACA. (b) Locations of Lake Harnur and Bayanbuluk meteorological station. White color denotes the glacier distribution. (c) Mean monthly precipitation (red histogram) and temperature (blue dot line) at Byanbuluk meteorological station (data from 1958 to 2008). (For interpretation of the references to colour in this figure legend, the reader is referred to the web version of this article.)

Table 1
Paleo-records mentioned in text over the central Asia. Also see site numbers in Fig. 1.

Site no.	Name	Lat. (°N)	Long. (°E)	Alt. (meter)	Proxies	Proxy indication	References
1	Caspian Sea	41.89	48.52	−24	Barrier complex	Lake level	Karpychev, 2001; Kroonenberg et al., 2007
2	Aral Sea	45.96	59.23	29	Diatom	Lake level	Austin et al., 2007; Sorrel et al., 2006; Boomer et al., 2009
3	Lake Sasikul	37.70	73.18	3816	Carbonate $\delta^{18}O$, TIC	Lake level/moisture	Lei et al., 2014
4	Lake Kalakuli	38.44	75.06	3650	Magentic susceptibility, Grain size, δD	Temperature and precipitation	Liu et al., 2014; Aichner et al., 2015
5	Lake Balkhash	46.54	74.86	338	Pollen	Precipitation	Feng et al., 2013
6	Lake Son kul	41.84	75.13	3014	Alkanes $\delta D_{n\text{-}C29}$	Precipitation/moisture	Lauterbach et al., 2014
7	W Tienshan tree ring	41.67	76.43	2700–3900	ring width	Temperature	Esper et al., 2002, 2003, 2007
8	Lake Issyk-kul	42.52	77.1	1603	Historical map	Lake level/precipitation	Narama, 2010
9	Kesang Cave	42.88	81.76	2070	Calcite $\delta^{18}O$	Precipitation	Cheng et al., 2012
10	Lake Ebinur	44.88	82.97	195	Carbonate $\delta^{18}O$, organic $\delta^{13}C$	Lake level/moisture	Ma et al., 2011
11	Lake Harnur	43.11	83.97	2941	Grain size	Temperature and precipitation	*This study*
12	Lake Manas	45.83	85.97	244	XRF and alkenone C_{37}	Lake level/moisture	Song et al., 2015
13	Lake Bosten	41.99	86.98	1048	Carbonate content	Moisture	Chen et al., 2006
14	Lake Bangongco	33.67	79.00	4241	Carbonate $\delta^{18}O$	Moisture	Fontes et al., 1996
15	Guliya ice core	35.28	81.48	6710	Net accumulation rate	Precipitation	Thompson et al., 1995; Yao et al., 1996
16	Keriya River	37.86	81.51	1350	Terrace	Precipitation	Yang et al., 2002a,b
17	Niya section	37.13	82.78	1371	Pollen, element composition	Moisture	Zhong et al., 2001, 2004
18	East Tarim Basin	39.77	88.38	816	Plant $\delta^{13}C$	Moisture	Liu et al., 2011
19	Lake Sugan	38.85	93.90	2793	Alkenone indices $U^{k'}_{37}$ and $\%C_{37:4}$	Temperature and precipitation	He et al., 2013
20	Dunde ice core	38.10	96.40	5325	Pollen	Moisture	Liu et al., 1998
21	Delingha tree ring	37.27	97.53	4000	Tree ring $\delta^{18}O$	Moisture	Wang et al., 2013
22	Lake Gahai	37.13	97.52	2848	Alkenone indices $U^{k'}_{37}$ and $\%C_{37:4}$	Temperature and precipitation	He et al., 2013
23	Badain Jaran	39.55	102.37	1300	Chloride concentrations	Recharge rate of groundwater/Moisture	Ma and Edmunds, 2006; Gates et al., 2008

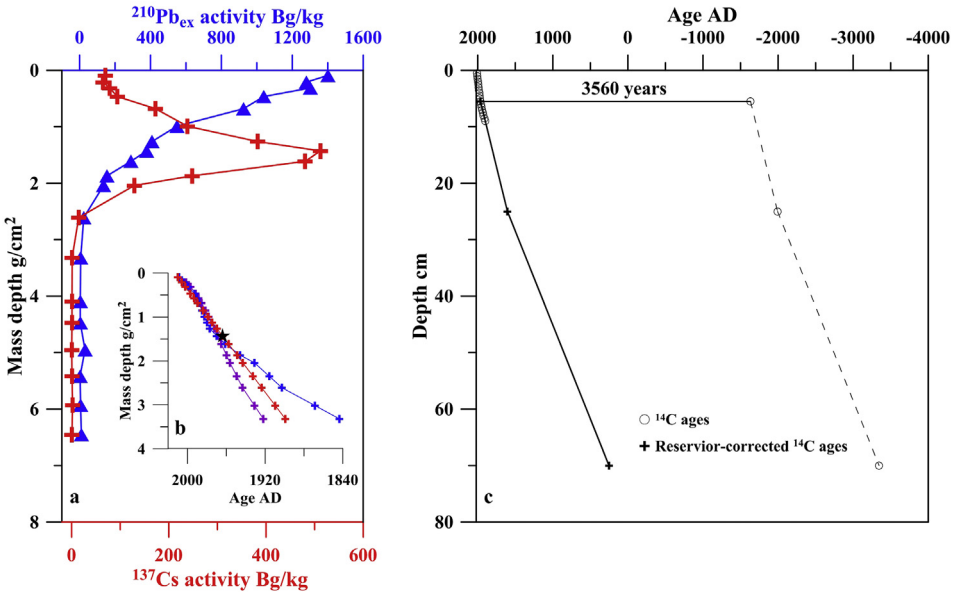

Fig. 2. (a) Surface sediments ^{137}Cs (blue) and $^{210}Pb_{ex}$ (red) activities of HENE13-1 core; (b) Age models of surface sediments: black star denotes the age of ^{137}Cs fallout deposition peak and the age model based on ^{137}Cs activity (red), and on constant initial concentration (purple) and constant rate of supply (blue) models. (c) Age model of HENE13-1 core. Age of the upper 9 cm sediments (0–9 cm) were derived from ^{137}Cs and ^{210}Pb dating, while those below 9 cm were calculated from the corrected ^{14}C ages (see text for details). (For interpretation of the references to colour in this figure legend, the reader is referred to the web version of this article.)

2. Study site

The Tianshan Mountain systems, which are the highest and largest elements of the central Asia mountain belt, extend from the east of Kyzylkum Desert in Uzbekistan, via Kazakhstan and Kirghizstan, to the Gobi/Desert at Hami, east of Xinjiang, China, with a total length of more than 2500 km, a width of 250–350 km and an average elevation of approximately 4000 m above sea level in China region (Hu, 2004). The Tianshan Mountain systems are divided into two branches in Xinjiang, and play an important role in defining regional climatic pattern (Aizen et al., 1997, 2001). The oases in central Asia are nurtured by rivers that originate from the Tianshan Mt., such as Syr-Darya River, Ili River, Tarim River, Kaidu River, Manas River, etc. Thus, climatic variations in Tianshan Mt. play a significant role in sustaining regional ecology, environment, and agriculture, etc.

Lake Harnur (43.11°N, 83.97°E, alt. 2941 m; maximum water depth: 29 m) is an open glacial lake, located in the central of south

Table 2
AMS^{14}C dating for sediment samples at Lake Harnur.

Sample No.	Lab ID	Depth (cm)	Uncalibrated ^{14}C age ± error (^{14}C yr BP)	Calibrated age, 1σ median probability (cal yr BP)	Calibrated reservoir-corrected ^{14}C Ages by 3560 Years (AD)
HENE13-1-11	XA11874	5.5	3341 ± 24	3583	1964
HENE13-1-50	XA12332	25	3631 ± 33	3943	1604
HENE13-1-140	XA11937	70	4571 ± 27	5295	252

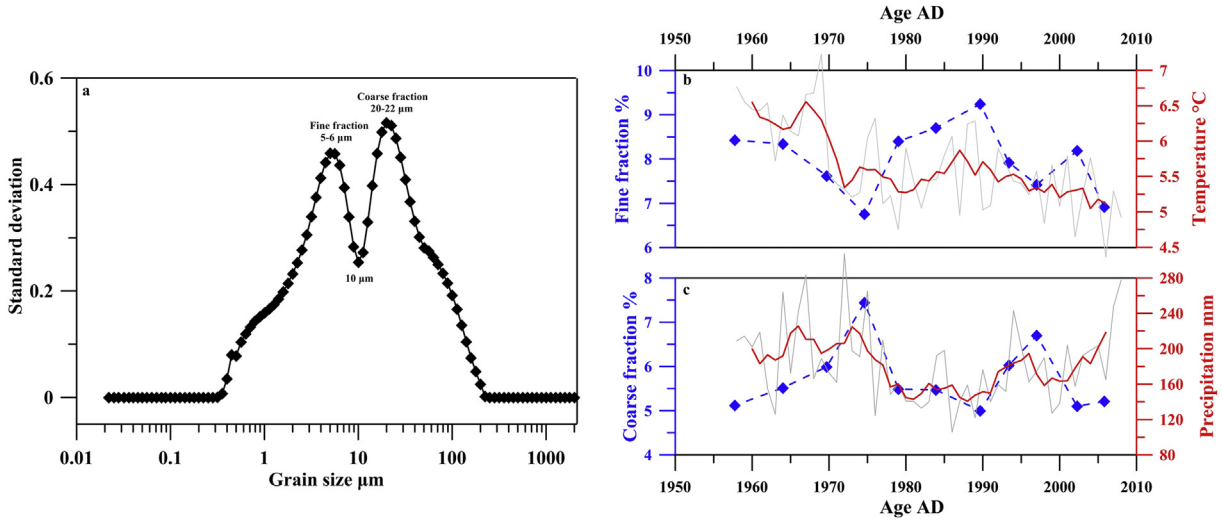

Fig. 3. Standard-deviation analysis of the sedimentary grain size in Lake Harnur (a), and comparison between the fine and coarse fractions (blue), with the mean ice-free seasons temperature (red solid line; 5-year running average; b) and the mean rainy seasons precipitation (red solid line; 5-year running average; c). (For interpretation of the references to colour in this figure legend, the reader is referred to the web version of this article.)

Tianshan Mt., with several streams originated from glacier in the high mountains (Fig. 1). Extending 1.6 km in length and 0.5 km in width, Lake Harnur covers a surface area of ~0.5 km^2 and a catchment of ~20 km^2. The lake is an oligotrophic, cold-water lake and has a mean salinity of 0.09 g/L and a mean pH of 6.20 (measured by YSI-6600 Z2 in 2013 and 2016).

Located in the Eurasian temperate continental high-alpine climatic conditions, Lake Harnur is characterized by short temperate summers and severely cold winters with ice cover usually between late October and early April. The long-term mean annual air temperature is about −4.3 °C, (recorded at Bayanbuluk meteorological station, 17 km southeastern of Lake Harnur; Fig. 1b and c), with January and July (coldest and warmest months) means of about −19.5 °C and 18.0 °C, respectively. The mean annual precipitation, which is mainly controlled by the interaction between the mid-latitude Westerlies and the Siberian Anticyclone (Aizen et al., 1997, 2001; 2006), is ~269 mm, with most of the precipitation occurring as convective rainfall during summer and less than 10% falls between October and March (Fig. 1c).

3. Materials and methods

In August 2013, we collected a surface sediment core from the center of Lake Harnur (HENE13-1; 70.0 cm long; water depth: 24 m) using a 60-mm UWITEC gravity corer (with 100% sediment recovery). The upper 5 cm of the cores are brown in color, while the rest of the sediments are gray in color. The HENE13-1 core was *in situ* sub-sampled at 0.5 cm intervals for the whole core, and was used to reconstruct the climate change in this study.

Radioactivities of Caesium-137 (^{137}Cs) and Lead-210 (^{210}Pb) of surface sediments (Fig. 2a) were measured on a multi-channel gamma spectrometry Ortec Germanium (HPGe) well detector (GWL-250-15) at Institute of Earth Environment, Chinese Academy of Sciences (IEECAS). To further constrain the chronology, three samples were dated by accelerator mass spectrometry (AMS) ^{14}C dating based on bulk organic matter (no plant debris was found in the sediments; Table 2) at the Xi'an AMS Center of IEECAS.

For grain size analysis, sediment samples were pretreated with 10% hydrogen peroxide (H_2O_2) and 30% hydrochloric acid (HCl) to remove the organic matter and carbonates, respectively (although Lake Harnur sediments contain only very limited amount of carbonates). The sedimentary of grain sizes were then determined using a Malvern Mastersizer 2000 laser particle size analyzer at IEECAS, with an analytical error of <3%.

4. Results

4.1. Chronology

4.1.1. ^{137}Cs and ^{210}Pb dating

^{137}Cs is an artificial radionuclide with a half-life of 30.17 years. After the nuclear weapon tests since 1945 AD, especially the worldwide nuclear tests during the 1950s, the concentration of ^{137}Cs rapidly increased, and globally peaked at 1963 AD in Northern Hemisphere (Pennington et al., 1973; Robbins and Edgington, 1975; Appleby, 2001). Although the Chernobyl nuclear accident at 1986 AD may have some influences on ^{137}Cs activities in lake sediments (Albrecht et al., 1998; Appleby, 2001; Eades et al., 2002; Klaminder et al., 2012), it is hard to be detected in most of the lake over the northwestern China (e.g., Zhang, 2005; Xu et al., 2010; Zhang et al., 2012; Yu et al., 2017). The ^{137}Cs activity of HENE13-1 core shows a classical pattern (Fig. 2a), with dramatic increase at the mass depth

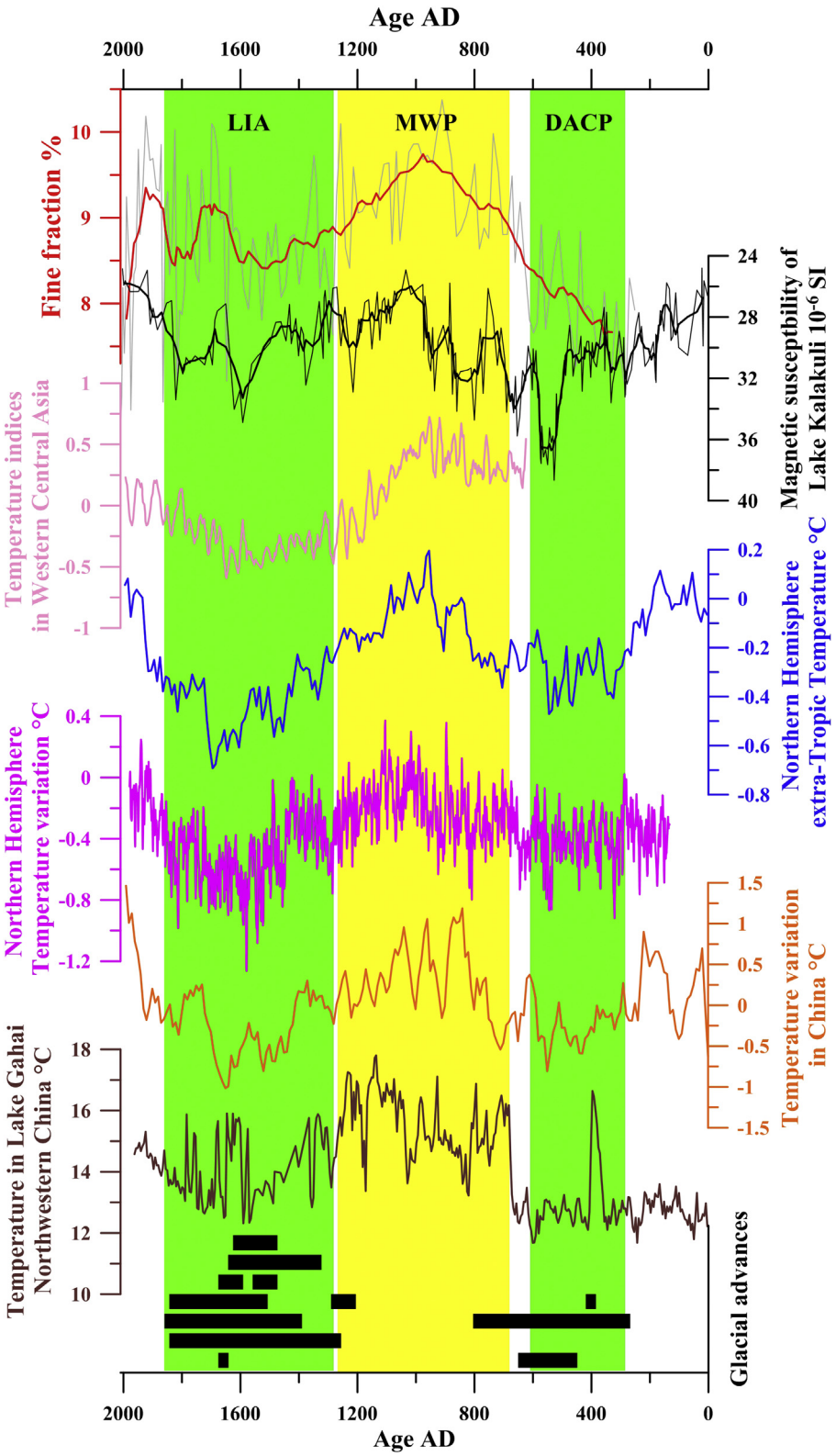

Fig. 4. Comparison between temperature changes in Lake Harnur (red; this study) and other temperature records from Pamir Plateau (black; Liu et al., 2014), Western central Asia (pink; Esper et al., 2002), extra-Tropical region of Northern Hemisphere (blue; Ljungqvist, 2010), Northern Hemisphere (Magenta; Moberg et al., 2005), China (orange; Yang et al., 2002a), Northwestern China (dark brown; He et al., 2013), and glacial advances of Tianshan Mt. (Li et al., 2014; Blomdin et al., 2016), Altai Mt. (Chernykh et al., 2013) and Pamir Plateau (Narama, 2002; Seong et al., 2009a, 2009b). (For interpretation of the references to colour in this figure legend, the reader is referred to the web version of this article.)

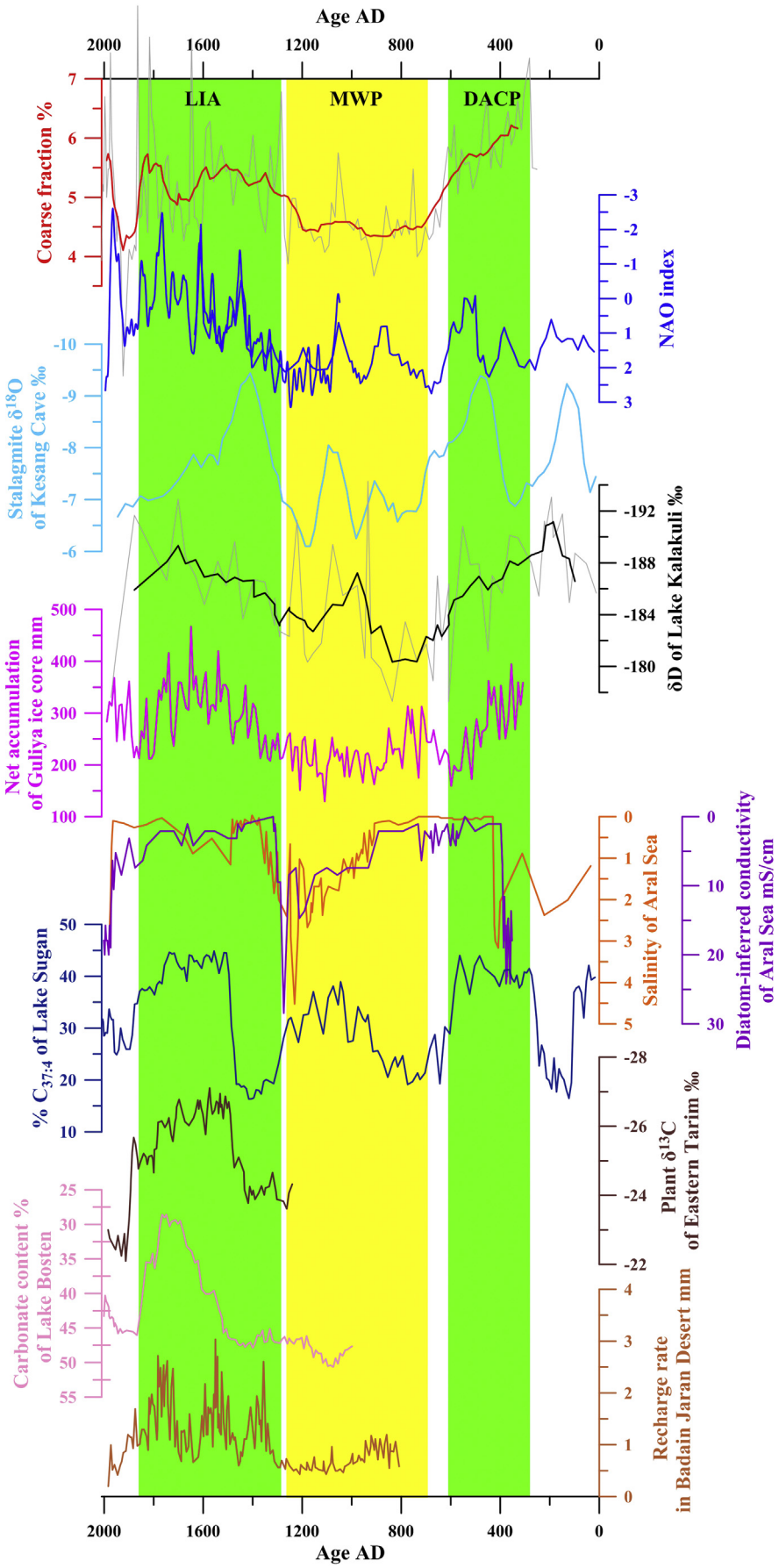
Age AD
2000
1600
1200
800
400
0
LIA
MWP
DACP
Coarse fraction %
NAO index
Stalagmite δ18O of Kesang Cave ‰
δD of Lake Kalakuli ‰
Net accumulation of Guliya ice core mm
Salinity of Aral Sea
Diatom-inferred conductivity of Aral Sea mS/cm
% C37:4 of Lake Sugan
Plant δ13C of Eastern Tarim ‰
Carbonate content % of Lake Bosten
Recharge rate in Badain Jaran Desert mm

of 2.04 g/cm^2 (the geometric depth of 7 cm), corresponding to the significant onset of the global ^{137}Cs fallout at 1952 AD (Yu et al., 2017). A unimodal ^{137}Cs peak (~510 Bq/kg) at the mass depth of 1.43 g/cm^2 (the geometric depth of 5.5 cm) is considered to be the maximum atmospheric radionuclide fallout deposition at 1963 AD, and the corresponding date is assigned as 1964 AD.

^{210}Pb is a natural radioactive nuclide in the Uranium-decay chains with a half-life of 22.23 years, and it has been widely used to establish dates of undisturbed sediment cores over the last 100–150 years (Appleby et al., 1979; Appleby, 2001; Sanchez-Cabeza and Ruiz-Fernandez, 2012). In this study, surface lake sediment dates (Fig. 2a and b) were determined according to both of the constant initial concentration (CIC) and the constant rate of supply (CRS) ^{210}Pb models (Robbins and Edgington, 1975; Appleby and Oldfield, 1978; Appleby et al., 1979), and both the CIC and CRS-ages are generally consistent with the ^{137}Cs-based ages since 1964 AD (Fig. 2b). Thus, the age model of the upper sediments is established based on a constant sedimentation rate inferred from the ^{137}Cs-^{210}Pb ages.

4.1.2. ^{14}C age model

The original AMS^{14}C ages are calibrated to calendar years before present with the program CALIB Revision 7.0.2 using the INTCAL 09 calibration data set (Stuiver and Reimer, 1993; Reimer et al., 2009). As shown in Fig. 2c and Table 2, the three radiocarbon ages show a generally linear correlation, suggesting a steady sedimentation rate. To evaluate the possible radiocarbon reservoir effect and/or systematic measurement error, we determine the ^{14}C age of the uppermost lake sediment at 5.5 cm (Liu et al., 2009, 2014; Xu et al., 2015), where the ^{137}Cs radioactivity peaked (corresponding to 1964 AD). The results suggest that the calibrated ^{14}C age of the sediment at the ^{137}Cs fallout peak is about 3560 years, deviated from the corresponding ^{137}Cs age (Table 2). A possible explanation is that the ^{14}C ages determined from bulk organic carbon are affected by old carbon effect, which is common in the radiocarbon dating of lacustrine sediments in the arid and semi-arid regions of western China (e.g., Liu et al., 2009; Mischke et al., 2010; Yu et al., 2014). Thus, we correct an old carbon effect of ~3560 years for all the three ^{14}C ages (Fig. 2c), and establish an integrated age model of core HENE13-1 based on the ^{137}Cs-^{210}Pb and AMS^{14}C dating results (Fig. 2c).

4.2. Standard-deviation analysis of grain size

The results of grain size analysis are demonstrated with grain size distribution curves or grain size parameters. The former is usually used to describe the contents of each grain size fraction; the latter mainly interprets sedimentary environment (Sun et al., 2003). However, the result of study in marginal sea (Sun et al., 2003) suggested that a single sample usually does not elucidate all grain size fractions in the sedimentary sequence; thus it is difficult to identify the sub-fractions. Therefore, all samples of Lake Harnur sediments are dealt with standard-deviation analysis to derive the sensitive grain size fractions (Boulay et al., 2003; Sun et al., 2003; Liu, 2016).

As shown in Fig. 3a, the distribution curve of grain size standard-deviation at Lake Harnur shows a bimodal pattern. The peak values of standard-deviation are clearly observed at 5–6 μm (fine fraction) and 20–22 μm (coarse fraction), which correspond to the modal grain size of each environmentally sensitive grain size fraction. The boundary of fine/coarse fraction grain size is around 10 μm (Fig. 3a).

5. Discussion

5.1. Grain size analysis and its implications

Grain size of lake sediments is widely used to reconstruct paleoclimate changes (Xiao et al., 2009; Huang et al., 2011; Xu et al., 2015, 2016; Gjerde et al., 2016; Nielsen et al., 2016). However, due to the different lake processes, the climatic significances of sedimentary grain size are variable, which three stand out. First, grain size is an indicator of lake level change (Xiao et al., 2009; Liu et al., 2016) and/or precipitation (Peng et al., 2005; Sheng et al., 2015; Xu et al., 2015, 2016), with larger (smaller) grain size indicating higher (lower) lake level and/or precipitation (Xu et al., 2015, 2016; Liu et al., 2016). Whereas, the completely opposite interpretation has also been suggested (Xiao et al., 2013, 2015). The second view proposes that grain size or coarse size content indicates the frequency of dust storms in arid and semi-arid region (Qiang et al., 2007; Huang et al., 2011; He et al., 2015). Third, in glacier lakes, grain size represents glacier activity or temperature change (Liu et al., 2014; Gjerde et al., 2016; Huang et al., 2016; Nielsen et al., 2016).

In this study, based on the standard-deviation method (Fig. 3a), two sensitive grain size fractions of Lake Harnur sediments are identified, which strongly point that the sediments of Lake Harnur have two sources. The first is the fine fraction (5–6 μm), which we speculate that it is captured into the high mountain glaciers of Lake Harnur catchment and then be transported to lake when glacier melt; thus its variation can indicate the change of glacier melt, which is primarily controlled by temperature changes. In fact, the size characteristic of ice core supports this viewpoint. For example, the size distribution of microparticles from Muztagata and Dunde ice core (Wu et al., 2009) is predominantly attributed to the particle between 3 and 15 μm, which contribute most (>70%) of the total volume. This characteristic of size distribution has also been reported from Tanggula ice core, central Tibetan Plateau (2–6 μm; Wu et al., 2013) and Greenland ice core (0.4–6 μm; Steffensen, 1997; Ruth et al., 2003). Therefore, we propose that the variation of fine fraction of Lake Harnur can serve as an indicator of regional temperature changes. The second is the coarse fraction (20–22 μm), for which we argue that it is mainly dominated by the runoff, directly responding to the precipitation changes. Thus, the variation of the coarse fraction can indicate the regional precipitation changes. We recognize that the surface runoff resulted from precipitation can also transport the fine fraction sediments into the lake, but its contribution is relatively constant and could have minor influence on the variability of the fine fraction.

To investigate these viewpoints further, we compare the fine fraction and the coarse fraction of the surface sediments with the mean ice-free seasons (April to October) temperature and the rainy seasons (June to August) precipitation from the nearest meteorological station, respectively (Fig. 3b and c). The results show that the variations of fine fraction are positively correlated with the ice-free seasons temperature changes (Fig. 3b), and the variations of coarse fraction are positively correlated with the rainy seasons precipitation changes (Fig. 3c). Therefore, these comparisons further support our viewpoints that the variations of fine and coarse fractions can

Fig. 5. Comparison of precipitation/moisture records from Lake Harnur (red; *this study*), NAO index (blue; Trouet et al., 2009; Olsen et al., 2012), Kesang Cave (sky blue; Cheng et al., 2012), Lake Kalakuli (black; Aichner et al., 2015), Guliya ice core (magenta; Thompson et al., 1995), Aral Sea (purple; Austin et al., 2007; orange, Sorrel et al., 2006), Lake Sugan (navy blue; He et al., 2013), Eastern Tarim (dark brown; Liu et al., 2011), Lake Bosten (pink; Chen et al., 2006), and Badain Jaran Desert (red brown; Ma and Edmunds, 2006). (For interpretation of the references to colour in this figure legend, the reader is referred to the web version of this article.)

indicate the change of regional temperature and precipitation, respectively.

5.2. Climate changes recorded at Lake Harnur over the past two millennia

Based on the interpretation of grain size at Lake Harnur sediments, we reconstruct the climate change over the past two millennia. As shown in Figs. 4 and 5, the record contains three typical stages on centennial time scale: Dark Age Period, Medieval Period, and Little Ice Age. The grain size shows that the low value of fine fraction and high value of coarse fraction during the Dark Age Period (~300–600 AD) were followed by the high value of fine fraction and low value of coarse fraction during the Medieval Period (700–1270 AD), which implied cold-wet climate conditions during the Dark Age Period, and warm-dry climate conditions during the Medieval Period. During the Little Ice Age (1300–1870 AD), the high-magnitude variation of grain size pointed to high frequency in climate changes. However, it still showed decreased temperature and increased precipitation on centennial time scale during the LIA. Overall, our record suggests a 'warm-dry and cold-wet' climate pattern at Lake Harnur on centennial time scale over the past two millennia.

Lake Harnur record also reveals the climate change on decadal to multi-decadal time scales. For example, there was an anomalously wet climate event around 1000 AD during the dry MWP (Fig. 5), which was also recorded in the surrounding areas, such as Kesang Cave (Cheng et al., 2012), Lake Kalakuli (Aichner et al., 2015), etc. Moreover, a relatively dry event occurred in the 16th during the wet LIA (Fig. 5), which was also documented at the ACA (Chen et al., 2010). However, considering the time resolution and dating uncertainty of our records, we do not deeply discuss the decadal to multi-decadal climate change in this study.

In addition, our records show a decouple of the 'warm-dry and cold-wet' climatic pattern during the current warm period (CWP; since ~1870 AD), which is possibly resulted from the reduced glacier-sourced fine fraction contribution due to the shrinkage of glacier under an unprecedented global warming.

5.3. Temperature changes of HCA over the past two millennia

Only few archives from the HCA could have recorded continuous temperature over the past two millennia. Glacier fluctuations of Muztagh Ata recorded in Lake Kalakuli from the Pamir Plateau correlated fairy well with temperature changes over China and Northern Hemisphere (Liu et al., 2014), showing significantly glacier retreat during the MWP and CWP, and glacier advance during the DACP and LIA (Fig. 4), and thus suggesting increased temperature during the MWP and CWP and decreased temperature during the DACP and LIA. These features were supported by tree-ring based temperature reconstructions from the western Tianshan Mt. (Fig. 4; Esper et al., 2002, 2003, 2007).

Moreover, a series of notable glacier advance events in the Tianshan Mt. (Fig. 4) also indicated decreased temperature during the LIA. For example, ^{10}Be surface exposure ages recorded the LIA glacier advance events in the eastern Tianshan Mt. (0.32 ± 0.08–0.43 ± 0.05 ka; Li et al., 2014; Blomdin et al., 2016), which coincide with those results from the western Tianshan Mt. (Savoskul and Solomina, 1996; Koppes et al., 2008). In the Altai and Pamir Plateau, dates of moraines suggested that there were a series of glacier advances during the DACP and LIA (Fig. 4). Based on the 17 radiocarbon dates from wood remains buried in moraines, Chernykh et al. (2013) demonstrated that glacier advances of Russian Altai took place in 400 AD, 1200–1300 AD and 1500–1850 AD, which is temporally similar with the LIA glacier advances reported by Zech et al. (2000) and Agatova et al. (2012). Investigations of Muztag Ata and Kongur Shan Mt. in Pamir Plateau also revealed glacier advances occurred during the DACP and LIA (Narama, 2002; Seong et al., 2009a, 2009b).

The satellite gravimetry, laser altimetry, and glaciological modelling show that temperature rather than precipitation is the main factor for controlling glacier retreats/advances of continental glacier (Du et al., 2008; Li, 2011; Li et al., 2011; Wang, 2012; Farinotti et al., 2015; Chen et al., 2016). As a result, the glacier advances during the DACP and LIA could be principally ascribed to regional temperature decreases. Further, comparisons of the reconstructed temperatures and/or glacier advances among Lake Harnur records (*this study*), tree ring records (Esper et al., 2002, 2003, 2007), lake records in the Pamir Plateau, and moraines records in the central Asia (Seong et al., 2009a, 2009b; Chernykh et al., 2013; Li et al., 2014; Blomdin et al., 2016) indicate an extensively similar temperature pattern in the HCA areas on centennial time scale (Fig. 4), which also suggest colder climatic conditions during the DACP and LIA.

We further compare temperature proxies of HCA with the reconstructed regional and global temperature changes over the past two millennia (Fig. 4). The results show that the centennial HCA temperature changes not only significantly correlate with those in China (Yang et al., 2002a) and northwestern China (He et al., 2013), but also with those in Northern Hemisphere (Moberg et al., 2005; Ljungqvist, 2010), implying that the centennial HCA temperature changes may have similar driving forces with those in Northern Hemisphere at least over the past two millennia, like solar forcing (Bond et al., 2001; Gray et al., 2010; Moffa-Sanchez et al., 2014) and volcanic eruption (Schurer et al., 2014; Sigl et al., 2015; Stoffel et al., 2015), etc.

5.4. Hydroclimatic changes in HCA areas over the past two millennia

Our record show increased precipitation during the DACP and LIA, whereas decreased during the MWP (Fig. 5), which is similar with the hydroclimatic pattern inferred from lines of biogeological evidence in HCA. For example, stalagmite $\delta^{18}O$ of Kesang Cave, 180 km western of Lake Harnur, showed relatively negative values during the DACP and LIA, whereas significantly positive values during the MWP (Cheng et al., 2012), suggesting wet climate conditions during the DACP and LIA and dry conditions during the MWP. Historical map from Lake Issyk-Kul, western Tianshan Mt., demonstrated a lower lake level during the MWP than modern lake, and substantially elevated lake level during the LIA (Narama, 2010), which is also supported by the sedimentary alkanes $\delta D_{n\text{-}C29}$ record in Lake Son kul (Lauterbach et al., 2014). High-resolution leaf wax δD records of Lake Kalakuli on Pamir Plateau also suggested a wet DACP and LIA, and a dry MWP (Aichner et al., 2015), which is in phase with results from Lake Sasikul, on Pamir Plateau (Lei et al., 2014).

Moreover, records from northern Tibet Plateau (also influenced by the westerlies) show similar precipitation/moisture trends to those over HCA areas on centennial time scale (Chen et al., 2010). For example, net ice accumulation rate of Guliya ice core indicated high precipitation during the DACP and LIA, whereas low in LIA (Thompson et al., 1995; Yao et al., 1996), which is roughly consistent with hydroclimatic conditions inferred from carbonate $\delta^{18}O$ of Lake Bangong Co, northwestern Tibet Plateau (Fontes et al., 1996), pollen records of Dunde ice core (Liu et al., 1998), and tree ring $\delta^{18}O$ of Delingha, northeastern Tibet Plateau (Wang et al., 2013).

Summarily, hydroclimatic changes at the Tianshan Mt., Pamir Plateau and northern Tibet Plateau suggest relatively wetter conditions during the cold periods (e.g., DACP, LIA), whereas drier

conditions during the warm period (e.g., MWP) on centennial time scale over the past two millennia, indicating a 'warm-dry and cold-wet' hydroclimatic pattern over the HCA areas.

5.5. Consistent of hydroclimatic pattern over the westerlies-dominated central Asia and its driving forces

Hydroclimatic pattern of ACA has a widely similar trend during the past ~1000 years, showing a dry MWP and a wet LIA based on lake sediments, ice cores, and aeolian sediments (Chen et al., 2010, 2015), and thus implying consistence of hydroclimatic changes between HCA and ACA over the past millennium (Fig. 5). For example, sea level variations of Caspian Sea reconstructed by the sand bars, bays and barrier complexes presented low sea level during the MWP and highstands during the LIA (Karpychev, 2001; Kroonenberg et al., 2007). Isotopic evidences of Lake Ebinur, northwestern China showed hydrological complexity over the past millennium, but still experienced a dry MWP and a wet LIA (Ma et al., 2011). Low lake level during the MWP and high lake level during the LIA were also supported by x-ray fluorescence and magnetic susceptibility data from Lake Manas, northwestern China (Song et al., 2015). Multi-proxy indices of Lake Bosten indicated a dry climate between 1000 and 1500 AD and a humid climate between 1500 and 1950 AD (Chen et al., 2006). Consistent and large negative isotopic excursions of plant remains from an aeolian sand sequence in arid eastern Tarim Basin strongly suggested a wetter climatic condition during the LIA (Liu et al., 2011). Both Keriya River (Yang et al., 2002b) and Niya area (Zhong et al., 2001, 2004) in southern Tarim Basin also showed increased precipitation during the LIA. Alkenone indices of Lake Sugan and Gahai, in Qaidam Basin, confirmed a dry MWP and a wet LIA (He et al., 2013). For the easternmost central Asia, groundwater recharge rate of Badain Jaran Desert indicated decreased precipitation during the MWP and substantially increased precipitation during the LIA (Ma and Edmunds, 2006; Gates et al., 2008).

Furthermore, nearly the whole westerlies-dominated central Asia, including both the low and high elevated areas, shows a similar hydroclimatic pattern over the past two millennia (Fig. 5). For example, radiocarbon dating results of deposits in the Agrakhan sand bar and bays of the eastern Caspian Sea coast suggested high sea level during the DACP (Karpychev, 2001). Diatom-based conductivity from the Aral Sea indicated lake level expansion at ~400–900 AD and ~1350–1850 AD, and severe lake level regression at ~900–1350 AD (Austin et al., 2007; Boomer et al., 2009), which is synchronous with the reconstructed lake salinity based on the dinoflagellate cyst (Sorrel et al., 2006) and the reconstructed lake level based on mineralization (Oberhänsli et al., 2011). Based on the alkenone indices of lake sediments in Qaidam Basin, He et al. (2013) suggested relatively high moisture ca. 300–600 AD and 1500–1870 AD, and low moisture between 600 and 1450 AD. Considering the dating uncertainties of lake sediments over the ACA areas, we argue that both Aral Sea and Qaidam Basin could have experienced wet climate conditions during the DACP and LIA and dry during the MWP, which are consistent with the hydroclimatic pattern over the HCA areas. Therefore, we propose that a 'warm-dry and cold-wet' hydroclimatic pattern prevailed in the westerlies-dominated central Asia on centennial time scale over the past two millennia, which is consistent with the pollen-based temperature and precipitation reconstruction at Lake Balkhash (Feng et al., 2013) and with the synthesis of late Holocene climate changes over the ACA areas using various paleoclimate archives (Yang et al., 2009).

Asian Summer Monsoon could unlikely penetrate into the central Asia during the late Holocene because of the low summer insolation over the Northern Hemisphere (Cheng et al., 2012). Firn/ice cores $\delta^{18}O$ from Altai Mt. (Belukha) and Tianshan Mt. (Inilchek glacier) revealed that precipitations in central Asia are mainly originated from Aral-Caspian Sea, Mediterranean and Black Seas, and North Atlantic Ocean (Aizen et al., 2006). Based on 145 meteorological station data, Aizen et al. (2001) revealed an inverse relationship between precipitation in central Asia and Northern Atlantic Oscillation index (NAO), with increased precipitation during the negative phase of the NAO and the southward shift of the westerlies, and vice visa. The results of Community Climate System Model (CCSM) suggested that the southward shift of the westerlies and then the strengthened cyclone activity over the North Atlantic Ocean and Mediterranean Sea during the LIA promoted to an increase of extreme precipitation events (Raible et al., 2007), and subsequently resulted in the elevated precipitation in central Asia (Chen et al., 2010). Furthermore, the negative phase of the NAO during the LIA (Fig. 5; Trouet et al., 2009; Olsen et al., 2012) favors increasing precipitation; meanwhile strengthened Siberian High (SH) reconstructed from Greenland ice core (Meeker and Mayewski, 2002) may also led to increasing precipitation as a consequence of the strengthened anticyclone activity. Decreased precipitation in central Asia during the MWP, however, should be attributed to the positive phase of the NAO and thus the northward shift of the westerlies (Fig. 5; Trouet et al., 2009; Olsen et al., 2012), and the weakened SH (Meeker and Mayewski, 2002).

Although the NAO index during the DACP did not significantly decrease (Olsen et al., 2012), it was relatively low compared with that during the MWP (Fig. 5). The obviously increased precipitation during the DACP at Lake Harnur, Lake Kalakuli, Kesang Cave, Guliya ice core, Aral Sea, and Lake Sugan, etc., pointed to a most likely negative phase of the NAO index; otherwise some other driving forces could be involved.

6. Conclusions

Based on grain size from a glacier lake (Lake Harnur) at the central of southern Tianshan Mt., we reconstruct the regional climate change over the past two millennia, showing increased precipitation during the DACP and LIA, whereas decreased precipitation during the MWP. Comparison between our record and a large number of other records in HCA areas shows an extended 'warm-dry and cold-wet' hydroclimatic pattern over the HCA areas, which can be even extended to almost the whole westerlies-dominated central Asia. We argue that the phase of the NAO, the location of the westerlies, and the strength of the Siberia High pressure should integrately impact the hydroclimatic changes over the central Asia areas.

Acknowledgements

We thank Dr. Yonatan Goldsmith for valuable comments and suggestions on this paper. This work was funded by the National Natural Science Foundation of China (Nos 41672169, 41473120 and 41502171).

References

Agatova, A.R., Nazarov, A.N., Nepop, R.K., Rodnight, H., 2012. Holocene glacier fluctuations and climate changes in the southeastern part of the Russian Altai (South Siberia) based on a radiocarbon chronology. Quat. Sci. Rev. 43, 74–93.
Aichner, B., Feakins, S.J., Lee, J.E., Herzschuh, U., Liu, X., 2015. High-resolution leaf wax carbon and hydrogen isotopic record of the late Holocene paleoclimate in arid Central Asia. Clim. Past 11, 619–633.
Aizen, V.B., et al., 1997. Climatic and hydrologic changes in the tien shan, central Asia. J. Clim. 10, 1393–1404.
Aizen, E.M., Aizen, V.B., Melack, J.M., Nakamura, T., Ohta, T., 2001. Precipitation and atmospheric circulation patterns at mid-latitudes of Asia. Int. J. Climatol. 21, 535–556.
Aizen, V.B., Aizen, E.M., Joswiak, D.R., Fujita, K., Takeuchi, N., Nikitin, S.A., 2006. Climatic and atmospheric circulation pattern variability from ice-core isotope/

geochemistry records (Altai, Tien Shan and Tibet). Ann. Glaciol. 43, 49–60.
Albrecht, A., Reiser, R., Lück, A., Stoll, J.-M.A., Giger, W., 1998. Radiocesium dating of sediments from lakes and reservoirs of different hydrological regimes. Environ. Sci. Technol. 32, 1882–1887.
Appleby, P.G., 2001. Chronostratigraphic techniques in recent sediments. In: Last, W.M., Smol, J.P. (Eds.), Tracking Environmental Change Using Lake Sediments: Basin Analysis, Coring, and Chronological Techniques. Springer Netherlands, Dordrecht, pp. 171–203.
Appleby, P.G., Oldfield, F., 1978. The calculation of Lead-210 dates assuming a constant rate of supply of unsupported ^{210}Pb to the sediment. Catena 5, 1–8.
Appleby, P.G., Oldfield, F., Thompson, R., Huttunen, P., Tolonen, K., 1979. ^{210}Pb dating of annually laminated lake sediments from Finland. Nature 280, 53–55.
Austin, P., Mackay, A., Palagushkina, O., Leng, M., 2007. A high-resolution diatom-inferred palaeoconductivity and lake level record of the Aral Sea for the last 1600 yr. Quat. Res. 67, 383–393.
Blomdin, R., Stroeven, A.P., Harbor, J.M., Lifton, N.A., Heyman, J., Gribenski, N., Petrakov, D.A., Caffee, M.W., Ivanov, M.N., Hattestrand, C., Rogozhina, I., Usubaliev, R., 2016. Evaluating the timing of former glacier expansions in the Tian Shan: a key step towards robust spatial correlations. Quat. Sci. Rev. 153, 78–96.
Bond, G., Kromer, B., Beer, J., Muscheler, R., Evans, M.N., Showers, W., Hoffmann, S., Lotti-Bond, R., Hajdas, I., Bonani, G., 2001. Persistent solar influence on North Atlantic climate during the Holocene. Science 294, 2130–2136.
Boomer, I., Wunnemann, B., Mackay, A.W., Austin, P., Sorrel, P., Reinhardt, C., Keyser, D., Guichard, F., Fontugne, M., 2009. Advances in understanding the late Holocene history of the Aral Sea region. Quat. Int. 194, 79–90.
Boulay, S., Colin, C., Trentesaux, A., Pluquet, F., Bertaux, J., Blamart, D., Buehring, C., Wang, P., 2003. Mineralogy and sedimentology of Pleistocene sediment in the south China sea (ODP site 1144). Proc. Ocean Drill. Program Sci. Results 184, 1–21.
Chen, F., Huang, X., Zhang, J., Holmes, J.A., Chen, J., 2006. Humid little ice age in arid central Asia documented by Bosten lake, Xinjiang, China. Sci. China Ser. D Earth Sci. 49, 1280–1290.
Chen, F.H., Chen, J.H., Holmes, J., Boomer, I., Austin, P., Gates, J.B., Wang, N.L., Brooks, S.J., Zhang, J.W., 2010. Moisture changes over the last millennium in arid central Asia: a review, synthesis and comparison with monsoon region. Quat. Sci. Rev. 29, 1055–1068.
Chen, J.H., Chen, F.H., Feng, S., Huang, W., Liu, J.B., Zhou, A.F., 2015. Hydroclimatic changes in China and surroundings during the medieval climate anomaly and little ice age: spatial patterns and possible mechanisms. Quat. Sci. Rev. 107, 98–111.
Chen, Y., Li, W., Deng, H., Fang, G., Li, Z., 2016. Changes in central Asia's water tower: past, present and future. Sci. Rep. 6, 35458.
Cheng, H., Zhang, P.Z., Spotl, C., Edwards, R.L., Cai, Y.J., Zhang, D.Z., Sang, W.C., Tan, M., An, Z.S., 2012. The climatic cyclicity in semiarid-arid central Asia over the past 500,000 years. Geophys. Res. Lett. 39, L01705.
Chernykh, D.V., Galakhov, V.P., Zolotov, D.V., 2013. Synchronous fluctuations of glaciers in the Alps and Altai in the second half of the Holocene. Holocene 23, 1074–1079.
Diaz, H.F., Trigo, R., Hughes, M.K., Mann, M.E., Xoplaki, E., Barriopedro, D., 2011. Spatial and temporal characteristics of climate in medieval times revisited. Bull. Am. Meteorol. Soc. 92, 1487–1500.
Du, W., Qin, X., Liu, Y., Wang, X., 2008. Variation of the Laohugou glacier No.12 in the qilian mountains. J. Glaciol. Geocryol. 30, 373–379.
Eades, L.J., Farmer, J.G., MacKenzie, A.B., Kirika, A., Bailey-Watts, A.E., 2002. Stable lead isotopic characterisation of the historical record of environmental lead contamination in dated freshwater lake sediment cores from northern and central Scotland. Sci. Total Environ. 292, 55–67.
Esper, J., Schweingruber, F.H., Winiger, M., 2002. 1300 years of climatic history for Western Central Asia inferred from tree-rings. Holocene 12, 267–277.
Esper, J., Shiyatov, S.G., Mazepa, V.S., Wilson, R.J.S., Graybill, D.A., Funkhouser, G., 2003. Temperature-sensitive Tien Shan tree ring chronologies show multi-centennial growth trends. Clim. Dyn. 21, 699–706.
Esper, J., Frank, D.C., Wilson, R.J.S., Buntgen, U., Treydte, K., 2007. Uniform growth trends among central Asian low- and high-elevation juniper tree sites. Trees Struct. Funct. 21, 141–150.
Farinotti, D., Longuevergne, L., Moholdt, G., Duethmann, D., Molg, T., Bolch, T., Vorogushyn, S., Guntner, A., 2015. Substantial glacier mass loss in the Tien Shan over the past 50 years. Nat. Geosci. 8, 716–722.
Feng, Z.D., Wu, H.N., Zhang, C.J., Ran, M., Sun, A.Z., 2013. Bioclimatic change of the past 2500 years within the Balkhash basin, eastern Kazakhstan, central Asia. Quat. Int. 311, 63–70.
Fontes, J.C., Gasse, F., Gibert, E., 1996. Holocene environmental changes in Lake Bangong basin (western Tibet) .1: chronology and stable isotopes of carbonates of a Holocene lacustrine core. Palaeogeogr. Palaeoclimatol. Palaeoecol. 120, 25–47.
Gates, J.B., Edmunds, W.M., Ma, J.Z., Sheppard, P.R., 2008. A 700-year history of groundwater recharge in the drylands of NW China. Holocene 18, 1045–1054.
Gjerde, M., Bakke, J., Vasskog, K., Nesje, A., Hormes, A., 2016. Holocene glacier variability and Neoglacial hydroclimate at Alfotbreen, western Norway. Quat. Sci. Rev. 133, 28–47.
Graham, N.E., Ammann, C.M., Fleitmann, D., Cobb, K.M., Luterbacher, J., 2011. Support for global climate reorganization during the “medieval climate anomaly”. Clim. Dyn. 37, 1217–1245.
Gray, L.J., Beer, J., Geller, M., Haigh, J.D., Lockwood, M., Matthes, K., Cubasch, U., Fleitmann, D., Harrison, G., Hood, L., 2010. Solar influences on climate. Rev. Geophys. 48, RG4001.
He, Y., Zhao, C., Song, M., Liu, W., Chen, F., Zhang, D., Liu, Z., 2015. Onset of frequent dust storms in northern China at~ AD 1100. Sci. Rep. 5, 17111.
He, Y., Zhao, C., Wang, Z., Wang, H., Song, M., Liu, W., Liu, Z., 2013. Late Holocene coupled moisture and temperature changes on the northern Tibetan Plateau. Quat. Sci. Rev. 80, 47–57.
Hu, J., 2004. Physical Geography of the Tianshan Mountains in China. China Environmental Sciences Press, Beijing, pp. 48–50.
Huang, L., Zhu, L.P., Wang, J.B., Ju, J.T., Wang, Y., Zhang, J.F., Yang, R.M., 2016. Glacial activity reflected in a continuous lacustrine record since the early Holocene from the proglacial Laigu Lake on the southeastern Tibetan Plateau. Palaeogeogr. Palaeoclimatol. Palaeoecol. 345, 37–45.
Huang, X., Oberhänsli, H., von Suchodoletz, H., Sorrel, P., 2011. Dust deposition in the Aral Sea: implications for changes in atmospheric circulation in central Asia during the past 2000 years. Quat. Sci. Rev. 30, 3661–3674.
IPCC, 2007. Climate Change 2007: the Physical Science Basis. Cambridge University Press, New York, pp. 1–996.
Karpychev, Y.A., 2001. Variations in the Caspian Sea level in the historic epoch. Water Resour. 28, 1–14.
Klaminder, J., Appleby, P., Crook, P., Renberg, I., 2012. Post-deposition diffusion of ^{137}Cs in lake sediment: implications for radiocaesium dating. Sedimentology 59, 2259–2267.
Koppes, M., Gillespie, A.R., Burke, R.M., Thompson, S.C., Stone, J., 2008. Late quaternary glaciation in the Kyrgyz tien shan. Quat. Sci. Rev. 27, 846–866.
Kroonenberg, S.B., Abdurakhmanov, G.M., Badyukova, E.N., Van der Borg, K., Kalashnikov, A., Kasirnov, N.S., Rychagov, G.I., Svitoch, A.A., Vonhof, H.B., Wesselingh, F.P., 2007. Solar-forced 2600 BP and little ice age highstands of the Caspian sea. Quat. Int. 173, 137–143.
Lauterbach, S., Witt, R., Plessen, B., Dulski, P., Prasad, S., Mingram, J., Gleixner, G., Hettler-Riedel, S., Stebich, M., Schnetger, B., Schwalb, A., Schwarz, A., 2014. Climatic imprint of the mid-latitude Westerlies in the Central Tian Shan of Kyrgyzstan and teleconnections to North Atlantic climate variability during the last 6000 years. Holocene 24, 970–984.
Lei, Y.B., Tian, L.D., Bird, B.W., Hou, J.Z., Ding, L., Oimahmadov, I., Gadoev, M., 2014. A 2540-year record of moisture variations derived from lacustrine sediment (Sasikul Lake) on the Pamir Plateau. Holocene 24, 761–770.
Li, Z., 2011. The Recent Studies and Applications of Urumqi Glacier No.1, Tianshan Mountains. China Meteorological Press, China. Beijing, pp. 1–230.
Li, Z., Li, H., Chen, Y., 2011. Mechanisms and simulation of accelerated shrinkage of continental glaciers: a case study of Urumqi Glacier No. 1 in eastern Tianshan, Central Asia. J. Earth Sci. 22, 423–430.
Li, Y.K., Liu, G.N., Chen, Y.X., Li, Y.N., Harbor, J., Stroeven, A.P., Caffee, M., Zhang, M., Li, C.C., Cui, Z.J., 2014. Timing and extent of Quaternary glaciations in the Tianger Range, eastern Tian Shan, China, investigated using Be-10 surface exposure dating. Quat. Sci. Rev. 98, 7–23.
Liu, J., Wang, Y., Li, T.D., Tian, F., Yang, J.S., 2016. Comparison of grain-size distributions between nearshore sections and a deep-water sediment core from Dali Lake, North China, and inferred Holocene lake-level changes. J. Paleolimnol. 56, 123–135.
Liu, K.B., Yao, Z.J., Thompson, L.G., 1998. A pollen record of Holocene climatic changes from the Dunde ice cap, Qinghai-Tibetan Plateau. Geology 26, 135–138.
Liu, W.G., Liu, Z.H., An, Z.S., Wang, X.L., Chang, H., 2011. Wet climate during the 'little ice age' in the arid Tarim Basin, northwestern China. Holocene 21, 409–416.
Liu, X., 2016. High-resolution Climate Change on the Chinese Loess Plateau since the Last Deglaciation. PhD thesis. University of Chinese of Acadamy of Sciences, Beijing, pp. 1–125.
Liu, X., Dong, H., Yang, X., Herzschuh, U., Zhang, E., Stuut, J.W., Wang, Y., 2009. Late Holocene forcing of the Asian winter and summer monsoon as evidenced by proxy records from the northern Qinghai–Tibetan Plateau. Earth Planet. Sci. Lett. 280, 276–284.
Liu, X., Herzschuh, U., Wang, Y., Kuhn, G., Yu, Z., 2014. Glacier fluctuations of Muztagh Ata and temperature changes during the late Holocene in western-most Tibetan Plateau, based on glaciolacustrine sediment records. Geophys. Res. Lett. 41, 6265–6273.
Ljungqvist, F.C., 2010. A new reconstruction of temperature variability in the extra-Tropical Northern Hemisphere during the last two millennia. Geogr. Ann. Ser. A Phys. Geogr. 92A, 339–351.
Ma, J.Z., Edmunds, W.M., 2006. Groundwater and lake evolution in the Badain Jaran desert ecosystem, Inner Mongolia. Hydrogeol. J. 14, 1231–1243.
Ma, L., Wu, J., Yu, H., Haiao, Z., Abuduwaili, J., 2011. The medieval warm period and the little ice age from a sediment record of lake Ebinur, northwest China. Boreas 40, 518–524.
Meeker, L.D., Mayewski, P.A., 2002. A 1400-year high-resolution record of atmospheric circulation over the North Atlantic and Asia. Holocene 12, 257–266.
Mischke, S., Rajabov, I., Mustaeva, N., Zhang, C.J., Herzschuh, U., Boomer, I., Brown, E.T., Andersen, N., Myrbo, A., Ito, E., Schudack, M.E., 2010. Modern hydrology and late Holocene history of Lake Karakul, eastern Pamirs (Tajikistan): a reconnaissance study. Palaeogeogr. Palaeoclimatol. Palaeoecol. 289, 10–24.
Moberg, A., Sonechkin, D.M., Holmgren, K., Datsenko, N.M., Karlen, W., 2005. Highly variable Northern Hemisphere temperatures reconstructed from low- and high-resolution proxy data. Nature 433, 613–617.
Moffa-Sanchez, P., Born, A., Hall, I.R., Thornalley, D.J.R., Barker, S., 2014. Solar forcing of North Atlantic surface temperature and salinity over the past millennium. Nat. Geosci. 7, 275–278.

Narama, C., 2002. Late Holocene variation of the raigorodskogo glacier and climate change in the Pamir-Alai, central Asia. Catena 48, 21–37.
Narama, C., 2010. The lake-level changes in Central Asia during the last 1000 years based on historical map. In: Proceedings of International Workshop on "Reconceptualizing Cultural and Environmental Change in Central Asia: an Historical Perspective on the Future", 2010, Research Institute for Humanity and Nature, pp. 11–27.
Neukom, R., Gergis, J., Karoly, D.J., Wanner, H., Curran, M., Elbert, J., Gonzalez-Rouco, F., Linsley, B.K., Moy, A.D., Mundo, I., Raible, C.C., Steig, E.J., van Ommen, T., Vance, T., Villalba, R., Zinke, J., Frank, D., 2014. Inter-hemispheric temperature variability over the past millennium. Nat. Clim. Change 4, 362–367.
Nielsen, P.R., Balascio, N.L., Dahl, S.O., Jansen, H.L., Storen, E.W.N., Bradley, R.S., 2016. A high-resolution 1200-year lacustrine record of glacier and climate fluctuations in Lofoten, northern Norway. Holocene 26, 917–934.
Oberhänsli, H., Novotna, K., Piskova, A., Chabrillat, S., Nourgaliev, D.K., Kurbaniyazov, A.K., Matys Grygar, T., 2011. Variability in precipitation, temperature and river runoff in W Central Asia during the past similar to 2000 yrs. Glob. Planet. Change 76, 95–104.
Olsen, J., Anderson, N.J., Knudsen, M.F., 2012. Variability of the north Atlantic oscillation over the past 5,200 years. Nat. Geosci. 5, 808–812.
PAGES 2k Consortium, 2013. Continental-scale temperature variability during the past two millennia. Nat. Geosci. 6, 339–346.
Peng, Y.J., Xiao, J., Nakamura, T., Liu, B.L., Inouchi, Y., 2005. Holocene East Asian monsoonal precipitation pattern revealed by grain-size distribution of core sediments of Daihai Lake in Inner Mongolia of north-central China. Earth Planet. Sci. Lett. 233, 467–479.
Pennington, W., Tutin, T., Cambray, R., Fisher, E., 1973. Observations on lake sediments using fallout ^{137}Cs as a tracer. Nature 242, 324–326.
Qiang, M.R., Chen, F.H., Zhang, J.W., Zu, R.P., Jin, M., Zhou, A.F., Xiao, S., 2007. Grain size in sediments from Lake Sugan: a possible linkage to dust storm events at the northern margin of the Qinghai-Tibetan Plateau. Environ. Geol. 51, 1229–1238.
Raible, C.C., Yoshimori, M., Stocker, T.F., Casty, C., 2007. Extreme midlatitude cyclones and their implications for precipitation and wind speed extremes in simulations of the Maunder Minimum versus present day conditions. Clim. Dyn. 28, 409–423.
Reimer, P.J., Baillie, M.G.L., Bard, E., Bayliss, A., Beck, J.W., Blackwell, P.G., Bronk Ramsey, C., Buck, C.E., Burr, G.S., Edwards, R.L., Friedrich, M., Grootes, P.M., Guilderson, T.P., Hajdas, I., Heaton, T.J., Hogg, A.G., Hughen, K.A., Kaiser, K.F., Kromer, B., McCormac, F.G., Manning, S.W., Reimer, R.W., Richards, D.A., Southon, J.R., Talamo, S., Turney, C.S.M., van der Plicht, J., Weyhenmeyer, C.E., 2009. IntCal09 and Marine09 radiocarbon age calibration curves, 0–50,000 Years cal BP. Radiocarbon 51, 1111–1150.
Robbins, J.A., Edgington, D.N., 1975. Determination of recent sedimentation rates in Lake Michigan using Pb-210 and Cs-137. Geochim. Cosmochim. Acta 39, 285–304.
Ruth, U., Wagenbach, D., Steffensen, J., Bigler, M., 2003. Continuous record of microparticle concentration and size distribution in the central Greenland NGRIP ice core during the last glacial period. J. Geophys. Res. 108, 4098.
Sanchez-Cabeza, J.A., Ruiz-Fernandez, A.C., 2012. ^{210}Pb sediment radiochronology: an integrated formulation and classification of dating models. Geochim. Cosmochim. Acta 82, 183–200.
Savoskul, O.S., Solomina, O.N., 1996. Late-Holocene glacier variations in the frontal and inner ranges of the Tian Shan, central Asia. Holocene 6, 25–35.
Schurer, A.P., Tett, S.F.B., Hegerl, G.C., 2014. Small influence of solar variability on climate over the past millennium. Nat. Geosci. 7, 104–108.
Seong, Y.B., Owen, L.A., Yi, C.L., Finkel, R.C., 2009a. Quaternary glaciation of Muztag Ata and Kongur shan: evidence for glacier response to rapid climate changes throughout the late glacial and Holocene in westernmost Tibet. Geol. Soc. Am. Bull. 121, 348–365.
Seong, Y.B., Owen, L.A., Yi, C.L., Finkel, R.C., Schoenbohm, L., 2009b. Geomorphology of anomalously high glaciated mountains at the northwestern end of Tibet: Muztag Ata and Kongur Shan. Geomorphology 103, 227–250.
Sheng, E.G., Yu, K.K., Xu, H., Lan, J.H., Liu, B., Che, S., 2015. Late Holocene Indian summer monsoon precipitation history at Lake Lugu, northwestern Yunnan Province, southwestern China. Palaeogeogr. Palaeoclimatol. Palaeoecol. 438, 24–33.
Sigl, M., Winstrup, M., McConnell, J.R., Welten, K.C., Plunkett, G., Ludlow, F., Buntgen, U., Caffee, M., Chellman, N., Dahl-Jensen, D., Fischer, H., Kipfstuhl, S., Kostick, C., Maselli, O.J., Mekhaldi, F., Mulvaney, R., Muscheler, R., Pasteris, D.R., Pilcher, J.R., Salzer, M., Schupbach, S., Steffensen, J.P., Vinther, B.M., Woodruff, T.E., 2015. Timing and climate forcing of volcanic eruptions for the past 2,500 years. Nature 523, 543–549.
Song, M., Zhou, A.F., Zhang, X.N., Zhao, C., He, Y.X., Yang, W.Q., Liu, W.G., Li, S.H., Liu, Z.H., 2015. Solar imprints on Asian inland moisture fluctuations over the last millennium. Holocene 25, 1935–1943.
Sorrel, P., Popescu, S.M., Head, M.J., Suc, J.P., Klotz, S., Oberhansli, H., 2006. Hydrographic development of the Aral Sea during the last 2000 years based on a quantitative analysis of dinoflagellate cysts. Palaeogeogr. Palaeoclimatol. Palaeoecol. 234, 304–327.
Steffensen, J., 1997. The size distribution of microparticles from selected segments of the Greenland Ice Core Project ice core representing different climatic periods. J. Geophys. Res. 102, 26755–26763.
Stoffel, M., Khodri, M., Corona, C., Guillet, S., Poulain, V., Bekki, S., Guiot, J., Luckman, B.H., Oppenheimer, C., Lebas, N., Beniston, M., Masson-Delmotte, V., 2015. Estimates of volcanic-induced cooling in the Northern Hemisphere over the past 1,500 years. Nat. Geosci. 8, 784–788.
Stuiver, M., Reimer, P.J., 1993. Extend ^{14}C data base and revised calib 3.0 ^{14}C age calibration program. Radiocarbon 35, 215–230.
Sun, Y.B., Gao, S., Li, J., 2003. Preliminary analysis of grain-size populations with environmentally sensitive terrigenous components in marginal sea setting. Chin. Sci. Bull. 48, 184–187.
Thompson, L.G., Mosleythompson, E., Davis, M.E., Lin, P.N., Dai, J., Bolzan, J.F., Yao, T., 1995. A 1000 year climate ice-core record from the Guliya ice cap, China: its relationship to global climate variability. Ann. Glaciol. 21, 175–181.
Trouet, V., Esper, J., Graham, N.E., Baker, A., Scourse, J.D., Frank, D.C., 2009. Persistent positive North Atlantic oscillation mode dominated the medieval climate anomaly. Science 324, 78–80.
Wang, X., 2012. Response of Glacier Variation to Climate Change in the Southern Altai Mountains, during the Last 40 Years. Master thesis. Lanzhou University, Lanzhou, pp. 1–54.
Wang, W.Z., Liu, X.H., Xu, G.B., Shao, X.M., Qin, D.H., Sun, W.Z., An, W.L., Zeng, X.M., 2013. Moisture variations over the past millennium characterized by Qaidam Basin tree-ring δ^{18}O. Chin. Sci. Bull. 58, 3956–3961.
Wu, G., Yao, T., Xu, B., Tian, L., Zhang, C., Zhang, X., 2009. Volume-size distribution of microparticles in ice cores from the Tibetan Plateau. J. Glaciol. 55, 859–868.
Wu, G., Zhang, C., Xu, B., Mao, R., Joswiak, D., Wang, N., Yao, T., 2013. Atmospheric dust from a shallow ice core from Tanggula: implications for drought in the central Tibetan Plateau over the past 155 years. Quat. Sci. Rev. 59, 57–66.
Xiao, J., Chang, Z., Si, B., Qin, X., Itoh, S., Lomtatidze, Z., 2009. Partitioning of the grain-size components of Dali Lake core sediments: evidence for lake-level changes during the Holocene. J. Paleolimnol. 42, 249–260.
Xiao, J.L., Fan, J.W., Zhou, L., Zhai, D.Y., Wen, R.L., Qin, X.G., 2013. A model for linking grain-size component to lake level status of a modern clastic lake. J. Asian Earth Sci. 69, 149–158.
Xiao, J.L., Fan, J.W., Zhai, D.Y., Wen, R.L., Qin, X.G., 2015. Testing the model for linking grain-size component to lake level status of modern clastic lakes. Quat. Int. 355, 34–43.
Xu, H., Lan, J.H., Sheng, E.G., Liu, B., Yu, K.K., Ye, Y.D., Shi, Z.G., Cheng, P., Wang, X.L., Zhou, X.Y., Yeager, K.M., 2016. Hydroclimatic contrasts over Asian monsoon areas and linkages to tropical Pacific SSTs. Sci. Rep. 6, 33177.
Xu, H., Liu, X.Y., An, Z.S., Hou, Z.H., Dong, J.B., Liu, B., 2010. Spatial pattern of modern sedimentation rate of Qinghai Lake and a preliminary estimate of the sediment flux. Chin. Sci. Bull. 55, 621–627.
Xu, H., Zhou, X.Y., Lan, J.H., Liu, B., Sheng, E.G., Yu, K.K., Cheng, P., Wu, F., Hong, B., Yeager, K.M., Xu, S., 2015. Late Holocene Indian summer monsoon variations recorded at Lake Erhai, southwestern China. Quat. Res. 83, 307–314.
Yang, B., Braeuning, A., Johnson, K.R., Shi, Y.F., 2002a. General characteristics of temperature variation in China during the last two millennia. Geophys. Res. Lett. 29, 1324.
Yang, X.P., Zhu, Z.D., Jaekel, D., Owen, L.A., Han, J.M., 2002b. Late Quaternary palaeoenvironment change and landscape evolution along the Keriya River, Xinjiang, China: the relationship between high mountain glaciation and landscape evolution in foreland desert regions. Quat. Int. 97–8, 155–166.
Yang, B., Wang, J., Bräuning, A., Dong, Z., Esper, J., 2009. Late Holocene climatic and environmental changes in arid central Asia. Quat. Int. 194, 68–78.
Yao, T., Thompson, L., Qin, D., Tian, L., 1996. Variations in temperature and precipitation in the past 2 000 a on the Xizang (Tibet) Plateau–Guliya ice core record. Sci. China (Series D) 26, 348–353.
Yu, K., Xu, H., Lan, J., Sheng, E., Liu, B., Wu, H., Tan, L., Yeager, K.M., 2017. Climate change and soil erosion in a small alpine lake basin on the Loess Plateau, China. Earth Surf. Process. Landf. 42, 1238–1247.
Yu, S.Y., Cheng, P., Hou, Z.F., 2014. A caveat on radiocarbon dating of organic-poor bulk lacustrine sediments in arid China. Radiocarbon 56, 127–141.
Zech, W., Glaser, B., Ni, A., Petrov, M., Lemzin, I., 2000. Soils as indicators of the Pleistocene and Holocene landscape evolution in the Alay range (Kyrgystan). Quat. Int. 65–6, 161–169.
Zhang, X., 2005. Discussion on interpretations of ^{137}Cs depth distribution profiles of lake deposits. J. Mt. Sci. 23, 294–299.
Zhang, X., Long, Y., Wen, A., He, X., 2012. Discussion on applying ^{137}CS and ^{210}Pbex for lake sediment dating in China. Quat. Sci. 32, 430–440.
Zhong, W., Shu, Q., Xiong, H., 2001. Pollen assemblages of Niya section in southern Xinjiang and paleoenvironmental evolution. Geogr. Res. 20, 91–96.
Zhong, W., Tashpolat, Wang, L., Li, C., 2004. Process and characteristics of historical climate and environment changes in southern margin of Tarim Basin. J. Desert Res. 24, 261–267.